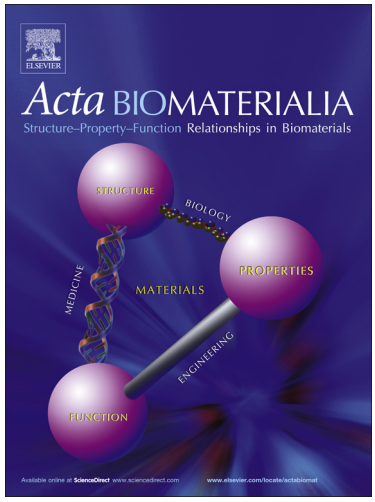

Full length article

Tuning acoustic and mechanical properties of materials for ultrasound phantoms and smart substrates for cell cultures

A. Cafarelli, A. Verbeni, A. Poliziani, P. Dario, A. Menciassi, L. Ricotti

PII: S1742-7061(16)30646-8
DOI: http://dx.doi.org/10.1016/j.actbio.2016.11.049
Reference: ACTBIO 4558

To appear in: *Acta Biomaterialia*

Received Date: 9 August 2016
Revised Date: 24 October 2016
Accepted Date: 21 November 2016

Please cite this article as: Cafarelli, A., Verbeni, A., Poliziani, A., Dario, P., Menciassi, A., Ricotti, L., Tuning acoustic and mechanical properties of materials for ultrasound phantoms and smart substrates for cell cultures, *Acta Biomaterialia* (2016), doi: http://dx.doi.org/10.1016/j.actbio.2016.11.049

Tuning acoustic and mechanical properties of materials for ultrasound phantoms and smart substrates for cell cultures

A. Cafarelli*, A. Verbeni, A. Poliziani, P. Dario, A. Menciassi, L. Ricotti

The Biorobotics Institute, Scuola Superiore Sant'Anna, Viale Rinaldo Piaggio 34, Pontedera (PI) 56025, Italy

Abstract

Materials with tailored acoustic properties are of great interest for both the development of tissue-mimicking phantoms for ultrasound tests and smart scaffolds for ultrasound mediated tissue engineering and regenerative medicine.
In this study, we assessed the acoustic properties (speed of sound, acoustic impedance and attenuation coefficient) of three different materials (agarose, polyacrylamide and polydimethylsiloxane) at different concentrations or cross-linking levels and doped with different concentrations of barium titanate ceramic nanoparticles.
The selected materials, besides different mechanical features (stiffness from few kPa to 1.6 MPa), showed a wide range of acoustic properties (speed of sound from 1022 to 1555 m/s, acoustic impedance from 1.02 to 1.67 MRayl and attenuation coefficient from 0.2 to 36.5 dB/cm), corresponding to ranges in which natural soft tissues can fall.
We demonstrated that this knowledge can be used to build tissue-mimicking phantoms for ultrasound-based medical procedures and that the mentioned measurements enable to stimulate cells with a highly controlled ultrasound dose, taking into account the attenuation due to the cell-supporting scaffold. Finally, we were able to correlate for the first time the bioeffect on human fibroblasts, triggered by piezoelectric barium titanate nanoparticles activated by low-intensity pulsed ultrasound, with a precise ultrasound dose delivered.
These results may open new avenues for the development of both tissue-mimicking materials for ultrasound phantoms and smart triggerable scaffolds for tissue engineering and regenerative medicine.

Keywords: Acoustic properties; mechanical properties; ultrasound phantoms; ultrasound cell stimulation; smart scaffolds.

1. Introduction

Tuning material physical properties is an effective way to engineer artificial or bioartificial systems for a wide range of biomedical applications. Materials with finely tuned features can indeed play a key role as synthetic replacements for biological tissues, substrates for tissue engineering, components of medical/surgical devices, drug delivery systems, diagnostic and array technologies and tissue-mimicking systems [1, 2]. In particular, material properties play a key role in two specific and rather distinct application domains, namely the development of tissue-mimicking phantoms for ultrasound (US) tests and the development of scaffolds for tissue engineering and regenerative medicine.

Tissue-mimicking phantoms are an important tool for performance testing and optimization of medical US systems and photoacoustic devices, as well as for medical training [3]. US phantoms must closely reflect the

* Corresponding author. Tel.: +39 050 883091.
E-mail address: a.cafarelli@sssup.it.

typical acoustic properties, such as speed of sound (SoS), acoustic impedance (Z) and attenuation coefficient (α) of natural tissues in order to reproduce US images similar to those obtained *in vivo* conditions.

US stimulation of cells and cell-seeded scaffolds has recently emerged as an intriguing tool to enhance certain cell responses in tissue engineering and regenerative medicine fields, by exploiting either direct mechanical effects [4, 5] or smart materials-based mediated ones [6, 7]. In this context, smart substrates can be defined as materials that are able to produce different types of stimuli (electrical, mechanical, thermal, chemical, etc.) and convey them to cells, once they are invested by a US wave.

Whenever an acoustic wave interacts with materials positioned within the propagation path, the material acoustic properties deeply influence the US attenuation or reflection and thus the US dose actually delivered to cells.

Therefore, an accurate knowledge of the acoustic properties (such as SoS, Z and α) of different materials is extremely useful both for the development of tissue-mimicking ultrasound phantoms and for the estimation of the effective dose to cells in ultrasound mediated tissue engineering applications.

In this study, three polymers were considered: agarose (AG), polyacrylamide (PAA) and polydimethylsiloxane (PDMS). They have been extensively used in both tissue-mimicking phantoms and tissue engineering/regenerative medicine fields.

In the field of tissue-mimicking phantoms, several materials were designed and characterized to be used as tissue-mimicking materials (TMMs) with the aim to tailor acoustic properties of tissues for specific applications in US-related medical fields [2].

The use of PDMS in this domain implies several advantages including stability, long-term duration and the possibility to mimic elastic properties of different tissues, making this material a valid solution for US phantoms in general and for elastography in particular. PDMS phantoms can be useful for surgical training, to simulate procedures such as biopsies and needle insertions and also for the development of new diagnostic strategies. However, silicone-like materials are usually discarded as TMMs for US phantoms, due to their high α (usually >2 dB/cm), low SoS (around 1000 m/s) and low Z (around 1 MRayl) [8] that make them rather different from natural soft tissues [9]. For the RT601 silicone, Zell *et al.* found a longitudinal SoS of 1030 m/s, a Z of 1.10 MRayl and an α of 14 dB/cm (at 7MHz) [3]. In a study focused on the estimation of ultrasonic shear rate in vascular applications, Tsou *et al.* [10] reported the longitudinal SoS and the α of PDMS at different formulations. It was found that PDMS acoustic properties are very different from biological tissues, but they can be adjusted by changing the monomer/curing agent ratio (*e.g.* by changing the ratio from 1:10 to 1:5, the SoS increased from 1076,5 up to 1119.5 m/s and the α decreased from 21.30 down to 14.86 dB/cm, at 5 MHz).

PAA shows very good acoustic properties and an acceptable stability over time, thus making it a good solution for US phantoms. A 10% PAA gel was used by Zell *et al.* [3]. The measured SoS (1580 m/s), Z (1.7 MRayl) were within a suitable range for mimicking soft tissues, while α (0.7 dB/cm at 5 MHz) resulted lower with respect to values shown by natural tissues. Prokop *et al.* proposed PAA gels at different concentrations as coupling media for focused ultrasound therapy [11]. Here, it was shown that acoustic properties varied linearly with acrylamyde concentration from 10% to 20% w/v: SoS ranged from 1546 to 1595 m/s, Z from 1.58 to 1.68 MRayl and α from 0.08 to 0.14 dB/cm, at 1 MHz.

PAA is also widely used for the fabrication of thermal phantoms, exploited, e.g., in the evaluation of high intensity focused ultrasound (HIFU) procedures [12, 13]. In these studies, PAA is commonly mixed with a thermosensitive material, such as bovine serum albumin (BSA) or egg-white, in order to become optically opaque when denatured [14, 15].

As reported by Culjat *et al.*, AG-based materials are widely used for US phantoms, due to the ease of fabrication, good acoustic (and mechanical) properties and the possibility to easily incorporate additional ingredients [2]. Therefore, AG-based materials have been rather well characterized in the previous literature [16].

The main AG acoustic properties, which are anyhow strongly influenced by material formulation and

manufacturing techniques, are the following: SoS in the range 1498–1600 m/s, α in the range 0.04–1.40 dB/cm and Z in the range 1.52–1.76 MRayls [17].

Cannon et al. developed AG-based materials for the production of a heterogeneous breast phantom, mimicking different anatomical structures of the breast (glandular tissue, subcutaneous fat, pectoral muscle, areola, malignant and benign lesions) under US [18]. In this study, the authors kept a constant concentration of AG (3% w/v) and modified the concentrations of different dopant agents (glycerol, silicon carbide and aluminum oxide) in order to slightly change the acoustic properties.

In addition to formulation, preparation conditions may play also an important role in determining the final properties of AG gels: Browne *et al.* found that AG SoS increases with increasing temperature by a rate of approximately 1.5 m s^{-1} $°C^{-1}$, while changes in α are negligible [19]; Ross and colleagues found that mixing conditions also strongly influence mechanical and acoustic properties of agar gels [20].

In the field of tissue engineering and regenerative medicine, PDMS, PAA and AG materials have been also extensively used, especially for mechanobiological studies. Substrate mechanical and (in some cases) surface chemical properties regulate in fact important cells behaviors such as adhesion, proliferation and differentiation [21-26].

In recent years the use of ultrasound as a therapeutic tool is a continuously expanding field and can find different applications in medicine including tissue ablation, regenerative medicine, gene therapy and targeted drug delivery [27, 28].

Scaffolds are commonly used to support cells also during US stimulation experiments, both *in vitro* and *in vivo*. However, a proper knowledge of their acoustic properties is almost always lacking. This hampers to estimate the actual US dose delivered to the target and, as a consequence, makes US exposure poorly repeatable: it has been demonstrated that the uncertainty on US exposure, during *in vitro* experiments, can be up to 700% [29].

No insights on acoustic properties of PDMS, PAA and AG materials intended for the development of cells substrates were reported.

To the best of our knowledge, a systematic analysis of acoustic characterization of PDMS, AG, PAA at different concentrations and cross-linking extents and doped with different concentrations of barium titanate ($BaTiO_3$) nanoparticles, has been not performed yet.

Ceramic $BaTiO_3$ nanoparticles were selected as filler because their presence in the matrix can modify the mechanical properties of the composite [30, 31]. In addition, although no specific data are available in the literature, they were expected to affect also the acoustic properties of the matrix, similarly to other ceramic materials [8, 17]. Finally, it is known that $BaTiO_3$ exhibits piezoelectric properties [32]. Therefore, when stimulated by US waves (mechanical inputs), they are able to generate local electrical charges that demonstrated to provide beneficial stimuli, thus enhancing cell adhesion, proliferation or differentiation [33].

Our hypothesis is that a precise measurement of such properties enables the development of tissue-mimicking phantoms and a highly controlled US exposure of living cells, thus overcoming the uncertainties connected with US wave attenuation and reflection, due to the scaffold on which cells are seeded.

Thus, in this paper we reported the acoustic characterization (speed of sound, acoustic impedance and attenuation measurements) of PDMS, AG and PAA and corresponding barium titanate-based nanocomposites.

We also reported two case studies; the former is a simplified tissue-mimicking phantom and the latter is a smart scaffold for controlled US stimulation of cells, with the aim of correlating the bioeffects triggered by the interaction between piezoelectric nanocomposites and US waves with a precise US dose delivered.

2. Materials and methods

2.1. Material preparation

AG samples were prepared by dissolving agarose powder (Sigma-Aldrich) in deionized and degassed water (dd-H_2O) at 6 different concentrations (2, 3, 4, 5.5, 6.5, 7.5 % w/v). Solutions were kept at 90° C for 1 h under continuous stirring and then cooled down at room temperature to allow material reticulation.

PAA gels were produced at 6 different concentrations by varying the percentages of acrylamide (A) and Bis-acrylamide (B-A) (Sigma-Aldrich) in dd-H_2O as follows: PAA5% (5%A, 0.1%B-A w/v), PAA7% (7%A, 0.2%B-A w/v), PAA9% (9%A, 0.3%B-A w/v), PAA11% (11%A, 0.4%B-A w/v), PAA13% (13%A, 0.5%B-A w/v) and PAA15% (15%A, 0.6%B-A w/v). All samples were supplemented with 1/200 v/v of 10% ammonium persulfate (Sigma-Aldrich) and 0.15% v/v of N,N,N',N'-tetramethylethylenediamine (TEMED, Sigma-Aldrich) to promote crosslinking reactions.

PDMS samples (Sylgard 184, Dow Corning) were prepared in 6 different monomer/curing agent ratios (60:1, 50:1, 40:1, 30:1, 20:1, 10:1 w/w); the mixture was degassed under vacuum for 30 min, poured into proper molds and then thermally treated at 65°C, overnight.

Three additional formulations for each class of material were produced by doping the stiffest formulation (AG 7,5%, PAA 13% and PDMS 10:1) with barium titanate nanoparticles ($BaTiO_3$, 99.9% barium titanate, 100 nm of nominal size, Nanostructured & Amorphous Materials, Inc). $BaTiO_3$ nanoparticles were added in solution at 3 different concentrations (0.1, 1 and 10% w/v) before the reticulation process completed, to obtain homogeneous nanocomposites.

To overcome the issue of a rather poor nanoparticle dispersibility in aqueous solutions (for PAA and AG gels), they were first mixed with a 0.1% w/v glycol chitosan (Sigma-Aldrich) solution and sonicated overnight (2510, Bransonic sonicator). This treatment guaranteed a polymer wrapping around nanoparticles, which enhanced their dispersibility and long-term stability [34]. Then, the glycol chitosan-wrapped nanoparticles were used to prepare the composite samples. Figure 1 summarizes the different sample types prepared and tested in this study.

All material types were obtained through properly designed Teflon molds. Cylindrical specimens of diameter (d) = 30 mm and height (h) = 20 mm were used for acoustic tests.

Figure 1. Schematic representation of material formulations used for preparing the different sample types analyzed in this study.

2.2. Acoustic characterization

Material speed of sound (SoS) and attenuation coefficient (α) were measured by using an insertion technique (also referred as through-transmission technique), in which the unknown acoustic properties of the material under investigation were obtained from comparison with the properties of a reference material (*i.e.* water) [35]. The used experimental set-up is depicted in Figure 2a. The sample was positioned between a US transducer used as transmitter (WS75-2 or WS75-5, Ultran Group) and a needle hydrophone (0.2 mm, Precision Acoustics Ltd) used as receiver. dd-H_2O was used as coupling medium and reference material. Sample and hydrophone were aligned along the main axis of the US transducer in order to maximize the acquired signal.

The US transducer was driven by a wave generator (33220A, Agilent Technologies), connected in series with a 50 dB power amplifier (240L, Electronics & Innovation). A dedicated LabVIEW graphic user interface

allowed the remote control of the wave generator and its synchronization with an oscilloscope (7034B, InfiniiVision, Agilent Technologies), from which the hydrophone signal was acquired at a 40 MHz sampling frequency. For all measurements, signals were mediated 10 times in order to significantly reduce noise. At least 3 independent samples for each formulation were tested.

Material SoS was calculated according to Equation 1, where h is the sample thickness, Δt is the delay

$$SoS = \frac{h}{\Delta t + \frac{h}{SoS_w}} \quad (1)$$

between the time of flight measured in presence of the sample and the time of flight measured in absence of the sample. SoS in water (SoS_w) was calculated as a function of temperature, by using the polynomial interpolation proposed by Marzak [36]. For a simple evaluation of the time of flight, the US transducer (WS75-2) was driven with a pulse signal (250 ns width and 5 ns edge time) and the maximum peak of the acquired signal was considered for time of flight estimation. An example of the acquired signals for SoS measurements in presence and in absence of the sample is shown in Figure 2b.

Acoustic Impedance (Z) was calculated by multiplying SoS by material density (ρ), calculated as the ratio between sample mass and volume (Equation 2). Volume was assessed with a water-displacement technique [11], using a measurement sensitivity of 100 µL and using a Hirox microscope (Hi-scope KH-2700), mounted orthogonally to the liquid column in which the sample was immersed, to precisely discriminate volume changes.

$$Z = SoS * \rho \quad (2)$$

α was evaluated at 5 different frequencies (1, 2, 3, 4 and 5 MHz) using Equation 3, where A_m and A_w are the root mean square of the acquired signal when the US transducer (WS75-2 for frequency f=1,2,3 MHz and WS75-5 for f=4,5 MHz) was driven with a sinusoidal tone burst of 40 cycles at frequency f in presence and absence of the sample, respectively, and h is the sample thickness. Representative signals acquired in presence and absence of the sample and used for α estimation are shown in Figure 2c.

$$\alpha = \frac{20}{h}\log_{10}\left(\frac{A_m}{A_w}\right) \quad (3)$$

To validate the system, the SoS of castor oil (Eur. Pharm. Grade, Acros Organics), featured by well-established properties and commonly used as acoustic reference material [37], was measured. The castor oil SoS value resulted 1508.8 ± 2.8 m/s at 28.8 °C, while α values were 0.85 ± 0.22, 2.68 ± 0.16, 5.02 ± 0.55, 8.90 ± 0.32 and 12.22 ± 0.79 dB/cm for f=1,2,3,4 and 5 MHz, respectively. These values were in line with those ones reported in previous studies [38, 39], thus confirming the reliability of the described set-up.

Figure 2. (a) Scheme of the experimental set-up used for speed of sound (SoS) and attenuation (α) measurements. Examples of signals acquired for SoS (b) and α (c) evaluation: reference signals (corresponding to water) and sample signals are represented with black and red lines, respectively.

2.3. Tissue-mimicking phantom development and ultrasound imaging

In order to demonstrate the possible application of the tested materials as tissue-mimicking phantoms for US tests, a simplified cirrhotic liver phantom [40-42] was fabricated.

Typical echoes of US imaging are mainly caused by differences in the acoustic impedance of materials (Z_i) at their interfaces. Thus, in order to reproduce an echographic representation of the interface similar to that one of a real cirrhotic liver in presence of ascites, materials showing a reflection coefficient (γ_r, Equation 4) matching the one of the real tissues were selected.

$$\gamma_r = \left(\frac{Z_2 - Z_1}{Z_2 + Z_1} \right)^2 \quad (4)$$

The phantom was built by using two different AG formulations. The liver was made of AG 7.5% $BaTiO_3$ 10% and fabricated by reflecting the main anatomical features of the native tissues. To this aim, a dedicated mold developed through a 3D printer (3DSystem Projet HD 3000) was used. The upper layer of the phantom, mimicking the properties of the surrounding ascites, was made of AG 2% and obtained by dropping the agar solution on top of a AG 7.5% $BaTiO_3$ 10% substrate, previously casted in the mold. US images were acquired by using an Esaote CA430E conventional 2D imaging convex ultrasound probe (Esaote) with a curvature radius of 40 mm and a working frequency of 3.5–5 MHz, positioned perpendicular to the liver/ascites interface.

2.4. Cell cultures and ultrasound exposure experiments

In order to minimize the typical exposure errors due to the use of commercial plastic well plates [29], custom culture wells with a Teflon structure and a 20 µm US-transparent polystyrene film with cells cultured on it were used for ultrasound cell stimulation experiments. First, polystyrene membranes were coated with collagen, to maximize their cell adhesiveness. They underwent oxygen plasma treatment (50 sec, 50 W) (Plasma Cleaner, Gambetti s.r.l.) and subsequent incubation with a 100 µg/mL collagen solution (Sigma-Aldrich) for 6 hours at 37 °C. Before cell seeding, samples were sterilized through UV light irradiation for 30 min.

Normal human dermal fibroblasts (nHDFs, purchased from Lonza, cat. CC-2511) were used for cell stimulation experiments. Cells were cultured in standard medium composed of 90% Dulbecco's Modified Eagle's Medium (DMEM, Euroclone) supplemented with 10% Fetal Bovine Serum (FBS, Euroclone), 100 IU/mL penicillin (EuroClone), 100 mg/mL streptomycin (EuroClone) and 2 mM Lglutamine (Sigma-Aldrich). During culture, the cells were maintained at 37 °C in a saturated humidity atmosphere containing 95% air and 5% CO_2. nHDFs (passage, 10) were seeded on the collagen-coated polystyrene membranes at a density of 3,000 cells/cm^2. Twenty-four h after seeding, cells underwent ultrasonic stimulation.

To this purpose, the Teflon structures holding the cell-seeded polystyrene membranes were filled of culture medium, sealed with parafilm, immersed in dd-H_2O and stimulated using an unfocused immersion ultrasound transducer (WS75-2, Ultran Group) previously calibrated and driven by a 1 MHz sinusoidal signal in pulsed mode (10 ms of burst period and 20% of duty cycle). The exposure time was set to 3 min and three different intensities (spatial peak pulse average, in the target) within the typical exposure regime of Low Intensity Pulsed Ultrasound (LIPUS) stimulation, were used: 200 mW/cm^2, 800 mW/cm^2 and 1600 mW/cm^2. This exposure regime was previously demonstrated to be safe [43] and effective in enhancing the proliferation of fibroblasts already at 200 mW/cm^2 [44].

Two additional exposure experiments were performed by interposing two different attenuating materials (PDMS 10:1 and PDMS 10:1 $BaTiO_3$ 10%) between the transducer and the cells. The materials were put into contact with the bottom side of the polystyrene membrane (the opposite side respect to the one covered by cells). The two materials were featured by a thickness of 12 and 4 mm, respectively, in order to attenuate half of the US dose delivered (1600 mW/cm^2). The attenuation was properly calculated by exploiting the results of acoustic characterization, reported in the next sections. Overall, the US dose at the target, with the mentioned materials interposed, resulted 800 mW/cm^2. Overall, six sample types were compared in US cell stimulation experiments: (1) samples stimulated at 200 mW/cm^2, (2) samples stimulated at 800 mW/cm^2, (3) samples stimulated at 1600 mW/cm^2 , (4) samples stimulated at 1600 mW/cm^2 but with a 12 mm, PDMS 10:1 material interposed, thus resulting in an overall dose of 800 mW/cm^2, (5) samples stimulated at 1600 mW/cm^2 but with a 4 mm, PDMS 10:1 $BaTiO_3$ 10% material interposed, thus resulting in an overall dose of 800 mW/cm^2 and (6) untreated controls.

The bioeffects triggered by US exposure were evaluated 24 h after stimulation experiments. At this time-point, samples were analyzed in terms of DNA content, to quantify the cell proliferation rate. Samples were rinsed three times with PBS (Euroclone), then 500 µL of milli-Q H_2O were added for each sample. Proper cell lysates were then obtained by two freeze/thaw cycles and ultrasonication. The DNA content in the cell lysates was measured by using the PicoGreen kit (Thermo Fisher Scientific). The PicoGreen dye binds to DNA, and the resulting fluorescence intensity is directly proportional to the DNA concentration. 50 µL of each sample were loaded for quantification in each well of a 96-well black microplate, together with working buffer and PicoGreen dye solution (100 and 150 µL/well, respectively), prepared according to the manufacturer instructions. After 10 min of incubation in the dark at room temperature, fluorescence intensity was measured through a microplate reader (Victor X3, Perkin Elmer), using an excitation wavelength of 485 nm and an emission wavelength of 535 nm. Four independent samples were analyzed for each sample type and each sample was read in triplicate in the microplate.

At the same time-point, cell number and shape were also qualitatively investigated, by using calcein AM imaging (Molecular Probes, L3224). Briefly, after removing the culture medium, the samples were rinsed with PBS. Then, 2 µM calcein AM in PBS was added and samples were incubated at 37 °C for 20 min. The samples were finally observed with an inverted fluorescent microscope (Eclipse Ti, FITC/TRITC filters, Nikon) equipped with a cooled CCD camera (DS-5MC USB2, Nikon) and with a NIS Elements imaging software.

3. Results and Discussion

3.1. Acoustic Characterization

The results of SoS and Z measurements are reported in Figure 3. The average SoS values were in the range from 1490.0 to 1512.1 m/s for AG (Figure 3a), from 1514.2 to 1555.4 m/s for PAA (Figure 3c) and from 1021.6 to 1054.7 m/s for PDMS (Figure 3e).

There was a clear trend of SoS values, which increased in correspondence to more concentrated solutions or more cross-linked formulations for each class of material. By contrast, the presence of nanoparticles in the matrix generally resulted in a decrease of SoS values.

The average values of Z ranged from 1.490 to 1.643 MRayls for AG (Figure 3b), from 1.535 to 1.667 MRayls for PAA (Figure 3d) and from 1.017 to 1.129 MRayls for PDMS (Figure 3f), with greater values in correspondence to more concentrated or more cross-linked formulations, similarly to SoS results. Doped materials generally showed higher Z values in comparison with non-doped counterparts, with the exception of PAA samples.

Such results confirm previous findings [3, 9] and further expand the knowledge on acoustic properties of these material classes, by analyzing a broader formulation range and $BaTiO_3$ nanoparticle-based composites. The presence of $BaTiO_3$ reduced speed of sound. This may appear as counterintuitive, but it is confirmed by other studies reporting reduced SoS values for materials provided with metal or ceramic fillers, in comparison with non-doped controls [8]. A different trend can be observed for Z measurements, probably because the decreased speed of sound was compensated by the higher density values of nanocomposites. SoS and Z numerical values for all sample types are reported in Table S1 (AG), Table S2 (PAA) and Table S3 (PDMS).

Regarding α measurement, results are reported in Table 1 for AG, Table 2 for PAA and Table 3 for PDMS, for US frequencies ranging from 1 up to 5 MHz.

The measured α of non-doped AG and PAA materials are in-line with typical values of hydrogels [11, 17], with values smaller than 1 dB/cm. PDMS samples showed significantly higher α values in comparison with AG and PAA samples, up to 17.63 dB/cm (PDMS 20:1 @ 5MHz) and 36.48 dB/cm (PDMS 10:1 BaTiO3 10%, @5MHz). Although a trend was rather clear (α values increasing with material concentration), no statistically significant differences are always evident between different concentrations of non doped materials. Statistically significant differences were found almost between doped and non-doped materials, at high nanoparticle concentrations, demonstrating that the adjunction of $BaTiO_3$ statistically increases the attenuation coefficient of AG, PAA and PDMS. Doped materials showed in fact α values up to 10.46 dB/cm for AG (AG 7.5% $BaTiO_3$ 10%, @5MHz), 3.13 dB/cm for PAA (PAA 15% $BaTiO_3$ 10%, @5MHz) and 36.48 dB/cm (PDMS 10:1 $BaTiO_3$ 10%, @5MHz). The variation of acoustic properties due to $BaTiO_3$ nanoparticles had been never analyzed before. Figure S1, S2 and S3 show graphical representations of α measurements.

Figure 3. Speed of Sound (SoS) and Acoustic Impedance (Z) for the tested materials: (a) AG SoS; (b) AG Z; (c) PAA SoS; (d) PAA Z; (e) PDMS SoS; (f) PDMS Z. Gridded bars refer to samples doped with $BaTiO_3$ nanoparticles. At least 3 independent samples were tested for each sample type. *=p<0.05, **=p<0.01.

Table 1. Attenuation Coefficient α (average ± SD) for AG and related nanocomposites. At least 3 independent samples were tested for each sample type. Statistical comparisons refer to values on each column: each sample is compared with the one reported in the row immediately above. *=p<0.05, **=p<0.01.

MATERIAL FORMULATION	α (dB/cm)				
	1 MHz	2MHz	3MHz	4MHz	5MHz
AG 2%	0.18 ± 0.14	0.16 ± 0.12	0.23 ± 0.19	0.27 ± 0.11	0.26 ± 0.14
AG 3%	0.21 ± 0.16	0.22 ± 0.12	0.27 ± 0.11	0.43 ± 0.26	0.33 ± 0.22
AG 4%	0.27 ± 0.23	0.39 ± 0.25	0.35 ± 0.25	0.52 ± 0.30	0.32 ± 0.22
AG 5.5%	0.33 ± 0.22	0.40 ± 0.31	0.39 ± 0.18	0.62 ± 0.14	0.88 ± 0.30 (*)
AG 6.5%	0.28 ± 0.16	0.27 ± 0.20	0.33 ± 0.23	0.54 ± 0.20	0.78 ± 0.21
AG 7.5%	0.39 ± 0.19	0.47 ± 0.23	0.41 ± 0.17	0.76 ± 0.23	0.99 ± 0.16
AG 7.5% $BaTiO_3$ 0.1%	0.58 ± 0.32	0.55 ± 0.28	0.44 ± 0.32	0.97 ± 0.50	1.40 ± 0.35
AG 7.5% $BaTiO_3$ 1%	0.96 ± 0.61	1.48 ± 0.72 (*)	1.11 ± 0.62	1.75 ± 0.55 (*)	2.42 ± 0.93
AG 7.5% $BaTiO_3$ 10%	6.97 ± 1.03 (**)	6.76 ± 1.86 (**)	8.28 ± 2.15 (**)	9.38 ± 1.47 (**)	10.46 ± 1.22 (**)

Table 2. Attenuation Coefficient α (average ± SD) for PAA and related nanocomposites. At least 3 independent samples were tested for each sample type. Statistical comparisons refer to values on each column: each sample is compared with the one reported in the row immediately above. *=p<0.05.

MATERIAL FORMULATION	α (dB/cm)				
	1 MHz	2MHz	3MHz	4MHz	5MHz
PAA 5%	0.17 ± 0.15	0.32 ± 0.26	0.26 ± 0.17	0.36 ± 0.30	0.39 ± 0.26
PAA 7%	0.17 ± 0.12	0.26 ± 0.21	0.23 ± 0.17	0.25 ± 0.16	0.47 ± 0.35
PAA 9%	0.13 ± 0.08	0.19 ± 0.13	0.24 ± 0.18	0.35 ± 0.24	0.53 ± 0.41
PAA 11%	0.19 ± 0.10	0.28 ± 0.19	0.18 ± 0.11	0.26 ± 0.22	0.65 ± 0.47
PAA 13%	0.21 ± 0.12	0.23 ± 0.17	0.30 ± 0.16	0.43 ±0.30	0.42 ± 0.22
PAA 15%	0.25 ± 0.17	0.25 ± 0.20	0.24 ± 0.16	0.36 ± 0.22	0.61 ± 0.36
PAA 15% $BaTiO_3$ 0.1%	0.47 ± 0.17	0.49 ± 0.20	0.55 ± 0.41	0.97 ±0.55 (*)	1.65 ± 0.58 (*)
PAA 15% $BaTiO_3$ 1%	0.64 ± 0.26	0.53 ± 0.24	0.91 ± 0.51	1.15 ± 0.55	2.16 ± 0.57
PAA 15% $BaTiO_3$ 10%	0.70 ± 0.30	0.85 ± 0.40	1.81 ± 0.61	1.78 ± 0.59	3.13 ± 0.62

Table 3. Attenuation Coefficient α (average ± SD) for PDMS and related nanocomposites. At least 3 independent samples were tested for each sample type. Statistical comparisons refer to values on each column: each sample is compared with the one reported in the row immediately above. *=p<0.05, **=p<0.01.

MATERIAL FORMULATION	α (dB/cm)				
	1 MHz	2MHz	3MHz	4MHz	5MHz
PDMS 60:1	1.95 ± 0.31	3.88 ± 0.35	7.48 ± 0.84	11.12 ± 0.27	15.78 ± 0.39
PDMS 50:1	1.71 ± 0.39	4.56 ± 0.42	8.05 ± 0.56	11.52 ± 0.78	15.92 ± 1.12
PDMS 40:1	2.10 ± 0.42	4.94 ± 0.21	8.54 ± 0.54	12.49 ± 0.31	16.60 ± 0.51
PDMS 30:1	2.00 ± 0.36	4.78 ± 0.67	8.75 ± 0.73	12.60 ± 1.18	17.29 ± 1.04
PDMS 20:1	2.23 ± 0.21	5.55 ± 0.75	9.37 ± 0.53	13.57 ± 1.07	17.63 ± 0.89
PDMS10:1	2.35 ± 0.28	5.72 ± 0.48	9.53 ± 0.95	13.74 ± 1.02	16.58 ± 1.95
PDMS10:1 $BaTiO_3$ 0.1%	2.72 ± 0.55	6.19 ± 0.63	10.36 ± 0.59	14.20 ± 1.25	17.74 ± 1.53
PDMS 10:1 $BaTiO_3$ 1%	3.21 ± 0.22	7.52 ± 0.38 (*)	12.50 ± 0.35	17.34 ± 0.51 (*)	21.01 ± 1.40 (*)
PDMS10:1 $BaTiO_3$ 10%	6.73 ± 0.15 (**)	17.03 ± 0.31 (*)	22.99 ± 0.46 (**)	28.30 ± 2.00 (**)	36.48 ± 1.52 (**)

3.2. Development of ultrasound phantoms

The phantom, fabricated with AG 2% and AG 7.5% BaTiO3 10% (Figure 4a) showed a γ_r value (calculated by means of Equation 4) of 0.0024, which was close to the one that can be found at the liver/ascites interface (γ_r = 0.0013) [2, 40]. Therefore, the echo generated in correspondence to the boundary was expected to be similar to the in vivo one. Figure 4b and Figure 4c show echographic images obtained with natural tissues and with the phantom, respectively. The two images appear very similar, thus qualitatively demonstrating that the tested materials can be used to effectively reproduce the echoes generated at certain tissues' boundaries and, more in general, the acoustic behavior of different anatomical structures.

Figure 4. a) Representation of the AG-based phantom and the US imaging acquisition system. US scanner images of a real cirrhotic liver [42] (b) and US images of the liver phantom made of AG 2% and AG 7.5% BaTiO3 10% (c). Figure (b) is reproduced with permission of the American Institute of Ultrasound in Medicine (Copyright Clearance Center's permission).

As visible in Table 4, human tissues possess specific mechanical and acoustic features, showing in some cases minimal differences among them [2, 9, 25, 40, 41, 45, 46]. Materials used for the development of ultrasound phantoms should as much as possible faithfully replicate natural tissue acoustic properties. In addition, mechanical properties must be also reproduced in applications such as ultrasound elastography, needle insertion and other US-guided procedures.

Table 4. Acoustic and mechanical properties of some human tissues.

Tissue	Young's Modulus [kPa]	Density [kg/m^3]	Speed of Sound [m/s]	Acoustic Impedance [MRayl]	Attenuation Coefficient [dB/(cm MHz)]
Blood	/	1060	1584	1.68	0.2
Brain	1-4	1040	1560	1.62	0.6
Breast	1-3	1020	1510	1.54	0.75
Cardiac	10-15	1060	1576	1.67	0.52
Fat	0.5-3	950	1478	1.40	0.48
Liver	8-12	1060	1595	1.69	0.50
Diseased Liver	6-25	1050	1527	1.60	0.58
Marrow	0.5-1.5	/	1435	/	0.5
Muscle	10-20	1050	1547	1.62	1.09
Tendon	1300-1700	1670	1750	1.84	4.7
Air	/	1.2	330	0.0004	/
Water	/	1000	1480	1.48	0.0022

Although in recent years some ultrasound phantoms have been developed [2, 3], the majority of tissue substitutes have been modeled by means of homogeneous materials, which do not realistically mimic the *in vivo* scenario. The systematic analysis made in this work, concerning characterization of AG, PAA and PDMS samples at different concentrations and cross-linking extents and corresponding nanocomposites, represents an added value in this field, since it allows to properly reproduce the features of a rather wide range of soft tissues.

3.3. Controlled in vitro ultrasound cell exposure

It is widely known that stiffness plays an important role in promoting/inhibiting cell processes [47] and substrates used for cell cultures in the field of tissue engineering are normally developed by properly taking into account such factor. However, when biomaterials are used in combination with US waves, acoustic properties must be also precisely known in order to stimulate cells with a highly controlled US dose. In fact, the interfaces between the US transducer and the cells can determine reflections or attenuations which must be estimated, to provide cells with a known US dose. This aspect is largely neglected in tissue engineering and related fields, but it is crucial to obtain reliable results, when US stimulation is involved [48].

Figure 5 shows the results obtained 24 h after stimulation of nHDFs in a highly controlled and reliable way, through a dedicated US set-up. We stimulated cells at 1 MHz for 3 min, providing different US intensities (200 mW/cm^2, 800 mW/cm^2 and 1600 mW/cm^2). One sample type was stimulated at the maximum intensity (1600 mW/cm^2) but a 12 mm specimen made of PDMS 10:1 was interposed between the transducer and the cells. Due to the acoustic properties of the specimen (α = 2.35 db/cm @ 1MHz, Table 3), we predicted

that the US signal should be attenuated at half of its intensity, thus resulting in a net US stimulation to cells equivalent to 800 mW/cm^2.

Fluorescence images (Figure 5a) showed a clear positive correlation between US dose and fibroblast proliferation, while no evident differences were found between samples stimulated at 800 mW/cm^2 and the ones provided with the 12 mm - PDMS 10:1 specimen. This was confirmed by quantitative data on DNA content, shown in Figure 5b.

As reported by ter Haar [49], pulsed ultrasound may produce transient cavitation effect as well as a change in volume and pressure caused by bubbles formed in the liquid medium, which when hitting one another release energy that may break chemical bonds, thereby producing reactive free radicals and provoking chemical changes in the cells. A pressure change due to this stimulation regime may modify the permeability of the cellular membrane to calcium and sodium ions, thus increasing protein synthesis. Furthermore, organelles may be altered due to irradiation forces. These alterations are thought to be responsible for the enhanced cell proliferation observed.

The bioeffect triggered by US stimulation (enhanced proliferation, correlated with US intensity) matches with the evidences reported by de Oliveira and colleagues [44]. In comparison with this study we achieved more marked proliferation differences at 24 h, due to a wider stimulation intensity range. In addition, the mentioned study focused on I929 (murine) fibroblasts, while we analyzed the response of human dermal fibroblasts. Furthermore, we demonstrated that the knowledge on the acoustic properties of the material interposed between the transducer and the cells allowed to correctly predict the actual intensity delivered, and thus the triggered bioeffect. In fact, the DNA content of the 800 mW/cm^2 sample and the one of the 1600 → 800 mW/cm^2 (12 mm – PDMS 10:1) were statistically equal and their average values were really close (1.375 and 1.414 µg/mL, respectively).

Figure 5. (a) Fluorescence images of nHDFs stimulated at different US intensities. Images were acquired 24 h after US stimulation. (b) DNA content for the different sample types 24 h after US stimulation. *=p<0.05.

Another experiment aimed at assessing the potential of $BaTiO_3$-based nanocomposites as smart responsive substrates for cell culture was performed. In fact, $BaTiO_3$ nanoparticles show piezoelectric properties that can convey the mechanical stimuli provided by US waves in electrical ones, thus targeting a series of possible intriguing bioeffects [50]. With the aim to assess if the presence of piezoelectric nanoparticles could result in a different bioeffect on nHDFs, we compared the sample type stimulated at 800 mW/cm^2 with another one stimulated at 1600 mW/cm^2 but provided with a 4 mm specimen made of PDMS 10:1 $BaTiO_3$ 10% (α = 6.73 db/cm @ 1MHz, Table 3) interposed between the transducer and the cells. Due to the acoustic properties of the specimen, we predicted that the US signal should be attenuated at half of its intensity, thus resulting in a net US stimulation to cells equivalent to 800 mW/cm^2. In addition, the piezoelectric nanoparticles entrapped in the top part of the specimen were in direct contact with the bottom side of the 20 µm polystyrene membrane (the opposite side respect to the one covered by cells).

Results are shown in Figure 6: interestingly, the proliferation effect was clearly enhanced in the presence of the interposed material, although the net US doses provided to the cells were the same. This was probably due to the piezoelectric effect and the electric field generation mediated by $BaTiO_3$ nanoparticles, which had a significant effect despite the nanocomposite was not in direct contact with the cells.

Figure 6. (a) Fluorescence images of nHDFs stimulated with an US dose of 800 mW/cm2 (top image) and with a net dose of 800 mW/cm^2, due to the attenuation of a 4 mm specimen made of PDMS 10:1 BaTiO3 10% (bottom image). Images were taken 24 h after US stimulation; (b) DNA content 24 h after US stimulation for the two sample types. **=p<0.01.

Few scientific evidences have been recently reported on this topic. A proliferation increase of H9c2 cardiac-like cells was observed by the authors on nanocomposites of poly(lactic-co-glycolic) acid and $BaTiO_3$ nanoparticles [51]. However, no US stimulation was performed in this study. More recently, Marino and colleagues reported enhanced osteoblast (Saos-2 cells) differentiation on a resin-based $BaTiO_3$ nanoparticles-doped scaffold, due to US stimulation [52]. Genchi and colleagues demonstrated enhanced neuron (SH-SY5Y cells) differentiation on poly(vinylidene fluoride-trifluoroethylene) films doped with the same nanoparticle type and stimulated with US waves [53]. In all these studies, US stimulation was performed in a poorly controlled way and the actual dose reaching the cells was not accurately measured, making the triggered bioeffects poorly repeatable. The same consideration applies for different yet connected evidences, related to intracellular stimulation mediated by piezoelectric nanoparticles [13, 14]. This work quantifies for the first time the bioeffect triggered by piezoelectric nanoparticles stimulated by US waves, by relating such bioeffect to a precise US dose delivered. From a biological viewpoint, the main mechanisms responsible for such biological responses are still rather unclear. In our case, the generation of electrical charges during US stimulation, due to the piezoelectric features of the composite substrate, probably influences voltage-gated channels on cell membranes, thus modifying the permeability of the cellular membrane to calcium and sodium ions, which alter protein synthesis and lately cell proliferation. The generated electrical charges may be also responsible for an enhanced adsorption of proteins (e.g. available in the culture medium) on the substrate, another event which may have a role in the marked enhancement of cell proliferation.

Finally, it is worth mentioning that the different material compositions and doping extents described in this study imply a significant tuning of matrix mechanical properties (see Figure S4 Table S7, Table S8 and Table S9 in the Supplementary Material). This is relevant in the field of tissue-mimicking phantoms, since in some cases (such as ultrasound elastography [54] or US guided needle insertion procedures [55, 56]), mechanical properties play a key role. Mechanical properties are also of paramount importance in the field of tissue engineering and regenerative medicine. It is well-known, in fact, that matrix local stiffness strongly influences cell adhesion, proliferation and differentiation [47, 57, 58]: integrins, cadherins, and other adhesion molecules that form cell focal adhesions allow to transmit forces to substrates. However, a normal cell not only applies forces but also responds through cytoskeleton organization (and other cellular processes) to the resistance that the cell senses, with deep implications on the main cell functions.

4. Statistical methods

All results were reported as mean values ± standard error of the mean. Analysis of variance (1-way ANOVA) was used to identify statistically significant differences among different groups. A Student's t-test was performed for comparison between two groups. Significance was set at 5 %.

5. Conclusions

This paper reports the acoustic characterization (speed of sound, acoustic impedance and attenuation measurements) of three different materials (agarose, polyacrylamide and polydimethylsiloxane) at different concentrations or cross-linking levels and doped with different concentrations of barium titanate nanoparticles. We demonstrated that a precise characterization of such material classes can be useful for the development of custom heterogeneous ultrasound phantoms that mimic the features of real tissues under ultrasound monitoring and for controlled acoustic exposure biological experiments, with the aim of triggering specific bioeffects.

We demonstrated that a proper material acoustic characterization allows to correctly predict the precise US dose delivered to cells, and thus the bioeffect to be triggered. In addition, we quantified for the first time the

bioeffect on human fibroblasts triggered by piezoelectric nanoparticles stimulated by US waves, namely a significant increase of proliferation, by relating such bioeffect to a precise US dose delivered.

We also mentioned the importance of mechanical properties, which were also tuned, together with the acoustic ones, by changing material composition and doping.

Future efforts will aim at developing new materials covering broader ranges of both mechanical and acoustic features, in order to mimic a larger number of soft and hard tissues. In addition, new dopant agents could be investigated with the aim to slightly modify both mechanical and acoustic properties. The promising results regarding the bioeffects triggered by the interaction between piezoelectric nanocomposites and US waves could be also investigated further, in view of a possible clinical translation of these evidences.

Acknowledgements

This work was partly supported by the M2Neural project (Multifunctional Materials for Advanced Neural Interfaces, http://www.m2neural.eu) funded in the FP7 M-ERA. NET Transnational framework, and by the FUTURA project (Focused Ultrasound Therapy Using Robotic Approaches, http://www.futuraproject.eu/) funded in the FP7 EU framework. Grant agreement no. 611963.

References

[1] Langer R, Tirrell DA. Designing materials for biology and medicine. Nature 2004;428:487-92.
[2] Culjat MO, Goldenberg D, Tewari P, Singh RS. A review of tissue substitutes for ultrasound imaging. Ultrasound Med Biol 2010;36:861-73.
[3] Zell K, Sperl J, Vogel M, Niessner R, Haisch C. Acoustical properties of selected tissue phantom materials for ultrasound imaging. Phys Med Biol 2007;52:N475.
[4] Doan N, Reher P, Meghji S, Harris M. In vitro effects of therapeutic ultrasound on cell proliferation, protein synthesis, and cytokine production by human fibroblasts, osteoblasts, and monocytes. J Oral Maxillofac Surg 1999;57:409-19.
[5] Thakurta SG, Kraft M, Viljoen HJ, Subramanian A. Enhanced depth-independent chondrocyte proliferation and phenotype maintenance in an ultrasound bioreactor and an assessment of ultrasound dampening in the scaffold. Acta Biomater 2014;10:4798-810.
[6] Ciofani G, Danti S, D'Alessandro D, Ricotti L, Moscato S, Bertoni G, Falqui A, Berrettini S, Petrini M, Mattoli V. Enhancement of neurite outgrowth in neuronal-like cells following boron nitride nanotube-mediated stimulation. ACS nano 2010;4:6267-77.
[7] Ricotti L, Fujie T, Vazão H, Ciofani G, Marotta R, Brescia R, Filippeschi C, Corradini I, Matteoli M, Mattoli V. Boron nitride nanotube-mediated stimulation of cell co-culture on micro-engineered hydrogels. PLoS One 2013;8:e71707.
[8] Cafarelli A, Miloro P, Verbeni A, Carbone M, Menciassi A. Speed of sound in rubber-based materials for ultrasonic phantoms. Journal of Ultrasound 2016:1-6.
[9] Duck FA. Physical properties of tissues: a comprehensive reference book: London: Academic Press, San Diego; 1990.
[10] Tsou JK, Liu J, Barakat AI, Insana MF. Role of ultrasonic shear rate estimation errors in assessing inflammatory response and vascular risk. Ultrasound Med Biol 2008;34:963-72.
[11] Prokop AF, Vaezy S, Noble ML, Kaczkowski PJ, Martin RW, Crum LA. Polyacrylamide gel as an acoustic coupling medium for focused ultrasound therapy. Ultrasound Med Biol 2003;29:1351-8.
[12] Dabbagh A, Abdullah BJJ, Ramasindarum C, Kasim NHA. Tissue-mimicking gel phantoms for thermal therapy studies. Ultrason Imaging 2014;36:291-316.
[13] Choi MJ, Guntur SR, Lee KI, Paeng DG, Coleman A. A Tissue Mimicking Polyacrylamide Hydrogel Phantom for Visualizing Thermal Lesions Generated by High Intensity Focused Ultrasound. Ultrasound Med

Biol 2013;39:439-48.
[14] Lafon C, Zderic V, Noble ML, Yuen JC, Kaczkowski PJ, Sapozhnikov OA, Chavrier F, Crum LA, Vaezy S. Gel phantom for use in high-intensity focused ultrasound dosimetry. Ultrasound Med Biol 2005;31:1383-9.
[15] Cafarelli A, Mura M, Diodato A, Schiappacasse A, Santoro M, Ciuti G, Menciassi A. A computer-assisted robotic platform for Focused Ultrasound Surgery: Assessment of high intensity focused ultrasound delivery. Engineering in Medicine and Biology Society (EMBC), 2015 37th Annual International Conference of the IEEE: IEEE; 2015. p. 1311-4.
[16] Madsen EL, Zagzebski JA, Banjavie RA, Jutila RE. Tissue mimicking materials for ultrasound phantoms. Med Phys 1978;5:391-4.
[17] Burlew MM, Madsen EL, Zagzebski JA, Banjavic RA, Sum SW. A new ultrasound tissue-equivalent material. Radiology 1980;134:517-20.
[18] Cannon LM, Fagan AJ, Browne JE. Novel tissue mimicking materials for high frequency breast ultrasound phantoms. Ultrasound Med Biol 2011;37:122-35.
[19] Browne J, Ramnarine K, Watson A, Hoskins P. Assessment of the acoustic properties of common tissue-mimicking test phantoms. Ultrasound Med Biol 2003;29:1053-60.
[20] Ross K, Pyrak-Nolte L, Campanella O. The effect of mixing conditions on the material properties of an agar gel—microstructural and macrostructural considerations. Food Hydrocolloids 2006;20:79-87.
[21] Palchesko RN, Zhang L, Sun Y, Feinberg AW. Development of polydimethylsiloxane substrates with tunable elastic modulus to study cell mechanobiology in muscle and nerve. PLoS One 2012;7:e51499.
[22] Genchi GG, Ciofani G, Liakos I, Ricotti L, Ceseracciu L, Athanassiou A, Mazzolai B, Menciassi A, Mattoli V. A straightforward method for obtaining long term PDMS/muscle cell biohybrid constructs. Colloids Surf B Biointerfaces 2013;105:144-51.
[23] Wang P-Y, Tsai W-B, Voelcker NH. Screening of rat mesenchymal stem cell behaviour on polydimethylsiloxane stiffness gradients. Acta Biomater 2012;8:519-30.
[24] Engler AJ, Griffin MA, Sen S, Bönnemann CG, Sweeney HL, Discher DE. Myotubes differentiate optimally on substrates with tissue-like stiffness pathological implications for soft or stiff microenvironments. The Journal of cell biology 2004;166:877-87.
[25] Engler AJ, Sen S, Sweeney HL, Discher DE. Matrix elasticity directs stem cell lineage specification. Cell 2006;126:677-89.
[26] Ulrich TA, Jain A, Tanner K, MacKay JL, Kumar S. Probing cellular mechanobiology in three-dimensional culture with collagen–agarose matrices. Biomaterials 2010;31:1875-84.
[27] Escoffre J-M, Bouakaz A. Therapeutic ultrasound: Springer; 2016.
[28] Ricotti L, Cafarelli A, Iacovacci V, Vannozzi L, Menciassi A. Advanced micro-nano-bio systems for future targeted therapies. Current Nanoscience 2015;11:144-60.
[29] Leskinen JJ, Hynynen K. Study of factors affecting the magnitude and nature of ultrasound exposure with in vitro set-ups. Ultrasound Med Biol 2012;38:777-94.
[30] Mendes SF, Costa CM, Caparrós C, Sencadas V, Lanceros-Méndez S. Effect of filler size and concentration on the structure and properties of poly (vinylidene fluoride)/BaTiO3 nanocomposites. Journal of Materials Science 2012;47:1378-88.
[31] Huang X, Xie L, Hu Z, Jiang P. Influence of BaTiO 3 nanoparticles on dielectric, thermophysical and mechanical properties of ethylene-vinyl acetate elastomer/BaTiO 3 microcomposites. IEEE Transactions on Dielectrics and Electrical Insulation 2011;18:375-83.
[32] Galasso FS, Kestigan M. Barium Titanate, BaTiO3. Inorganic Syntheses: Nonmolecular Solids, Volume 30 1973:111-2.
[33] Ciofani G, Menciassi A. Piezoelectric nanomaterials for biomedical applications: Springer; 2012.
[34] Ciofani G, Ricotti L, Canale C, D'Alessandro D, Berrettini S, Mazzolai B, Mattoli V. Effects of barium titanate nanoparticles on proliferation and differentiation of rat mesenchymal stem cells. Colloids Surf B

Biointerfaces 2013;102:312-20.
[35] Bamber J. Attenuation and absorption. Physical Principles of Medical Ultrasonics, Second Edition 2005:93-166.
[36] Marczak W. Water as a standard in the measurements of speed of sound in liquids. J Acoust Soc Am 1997;102:2776-9.
[37] He P. Determination of ultrasonic parameters based on attenuation and dispersion measurements. Ultrason Imaging 1998;20:275-87.
[38] Timme R. Speed of sound in castor oil. J Acoust Soc Am 1972;52:989-92.
[39] Dunn F, Edmonds P, Fry W. Absorption and dispersion of ultrasound in biological media. Biological engineering 1969;205:332.
[40] Zhang D, Gong X-F. Experimental investigation of the acoustic nonlinearity parameter tomography for excised pathological biological tissues. Ultrasound Med Biol 1999;25:593-9.
[41] Mueller S, Sandrin L. Liver stiffness: a novel parameter for the diagnosis of liver disease. Hepat Med 2010;2:49-67.
[42] Tchelepi H, Ralls PW, Radin R, Grant E. Sonography of diffuse liver disease. J Ultrasound Med 2002;21:1023-32.
[43] Martin E. The Cellular Bioeffects of Low Intensity Ultrasound. Ultrasound 2009;17:214-9.
[44] de Oliveira RF, Oliveira D, Soares CP. Effect of low-intensity pulsed ultrasound on l929 fibroblasts. Arch Med Sci 2011;7:224-9.
[45] Arda K, Ciledag N, Aktas E, Arıbas BK, Köse K. Quantitative assessment of normal soft-tissue elasticity using shear-wave ultrasound elastography. Am J Roentgenol 2011;197:532-6.
[46] Sartori S, Chiono V, Tonda-Turo C, Mattu C, Gianluca C. Biomimetic polyurethanes in nano and regenerative medicine. Journal of Materials Chemistry B 2014;2:5128-44.
[47] Discher DE, Janmey P, Wang Y-l. Tissue cells feel and respond to the stiffness of their substrate. Science 2005;310:1139-43.
[48] Shaw A, ter Haar GR. Telling it like it is. Journal of therapeutic ultrasound 2013;1:1.
[49] Ter Haar G. Basic physics of therapeutic ultrasound. Physiotherapy 1978;64:100.
[50] Ciofani G, Danti S, Ricotti L, D'Alessandro D, Moscato S, Mattoli V. Applications of piezoelectricity in nanomedicine. Piezoelectric nanomaterials for biomedical applications: Springer; 2012. p. 213-38.
[51] Ciofani G, Ricotti L, Mattoli V. Preparation, characterization and in vitro testing of poly (lactic-co-glycolic) acid/barium titanate nanoparticle composites for enhanced cellular proliferation. Biomed Microdevices 2011;13:255-66.
[52] Marino A, Barsotti J, de Vito G, Filippeschi C, Mazzolai B, Piazza V, Labardi M, Mattoli V, Ciofani G. Two-photon lithography of 3D nanocomposite piezoelectric scaffolds for cell stimulation. ACS applied materials & interfaces 2015;7:25574-9.
[53] Genchi GG, Ceseracciu L, Marino A, Labardi M, Marras S, Pignatelli F, Bruschini L, Mattoli V, Ciofani G. P (VDF‐TrFE)/BaTiO3 Nanoparticle Composite Films Mediate Piezoelectric Stimulation and Promote Differentiation of SH‐SY5Y Neuroblastoma Cells. Advanced Healthcare Materials 2016.
[54] Zaleska-DorobiszA U, KaczorowskiB K, PawluśB A, PuchalskaB A, InglotB M. Ultrasound elastography–review of techniques and its clinical applications. Brain 2013;6:10-4.
[55] Whittaker S, Lethbridge G, Kim C, Keon Cohen Z, Ng I. An ultrasound needle insertion guide in a porcine phantom model. Anaesthesia 2013;68:826-9.
[56] Leibinger A, Forte AE, Tan Z, Oldfield MJ, Beyrau F, Dini D, y Baena FR. Soft Tissue Phantoms for Realistic Needle Insertion: A Comparative Study. Ann Biomed Eng 2015:1-11.
[57] Her GJ, Wu H-C, Chen M-H, Chen M-Y, Chang S-C, Wang T-W. Control of three-dimensional substrate stiffness to manipulate mesenchymal stem cell fate toward neuronal or glial lineages. Acta Biomater 2013;9:5170-80.
[58] Ricotti L, Menciassi A. Engineering stem cells for future medicine. Biomedical Engineering, IEEE

Transactions on 2013;60:727-34.

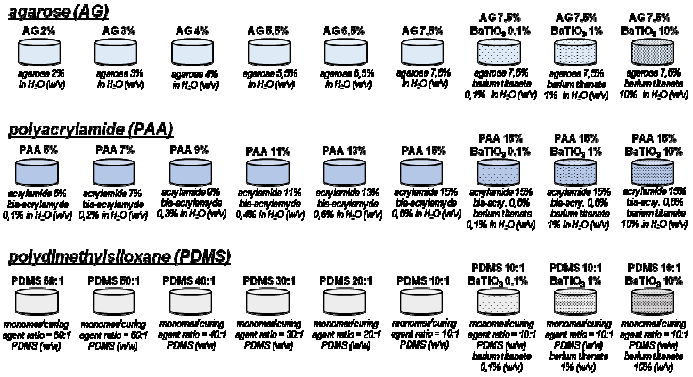

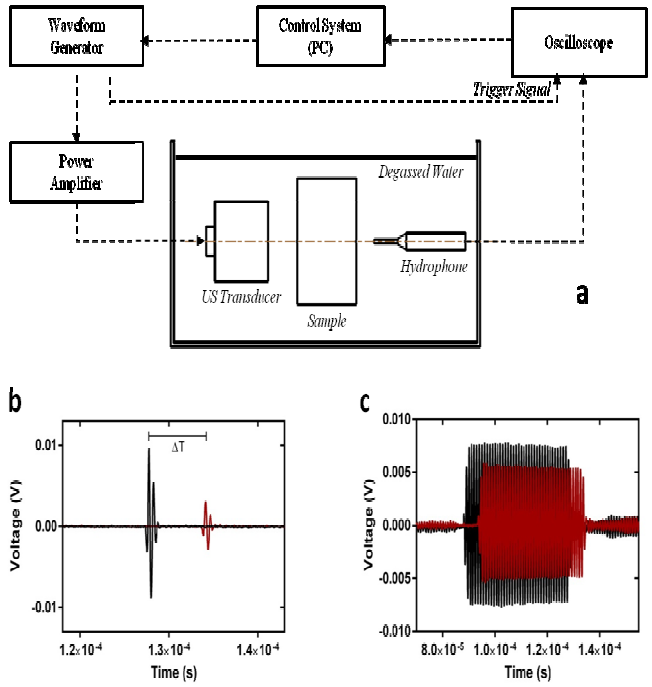

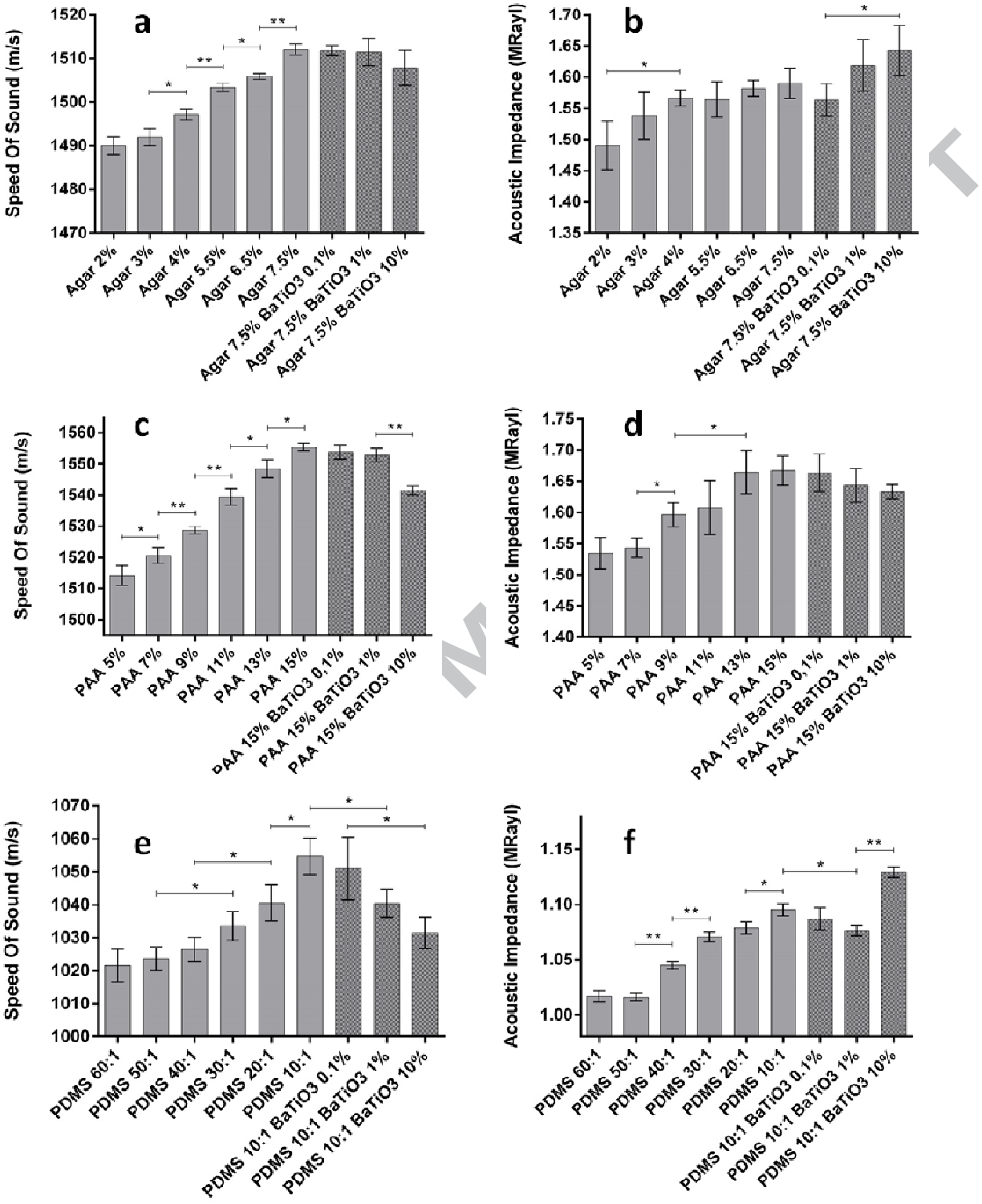

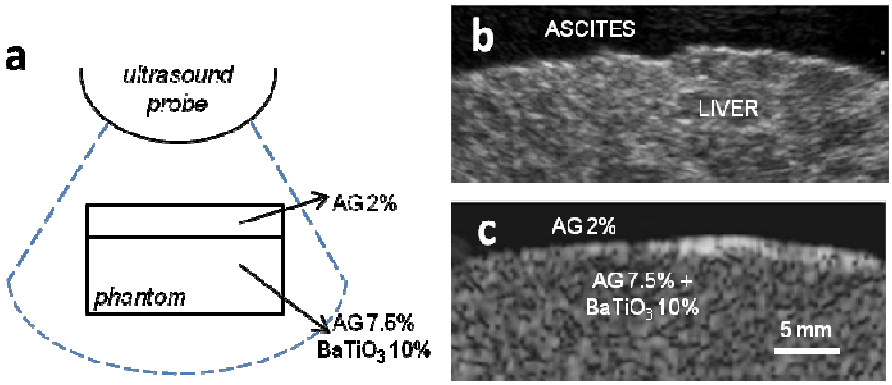

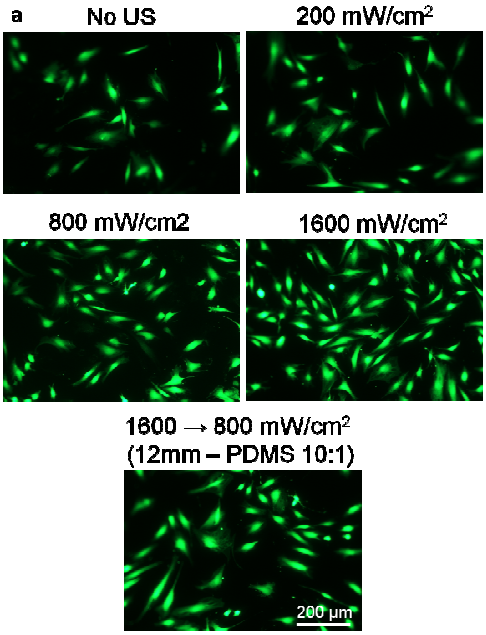

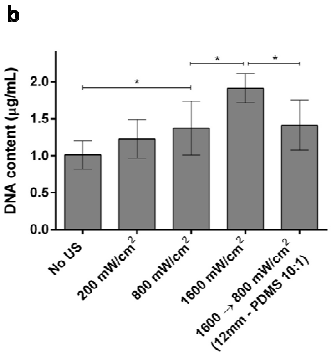

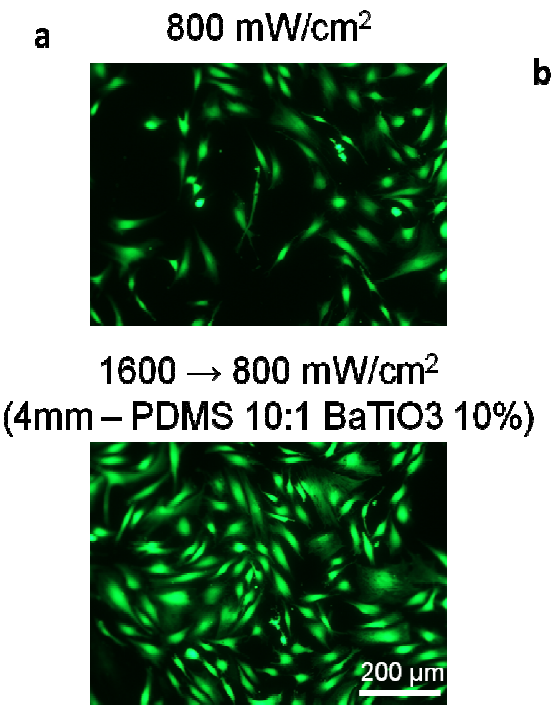

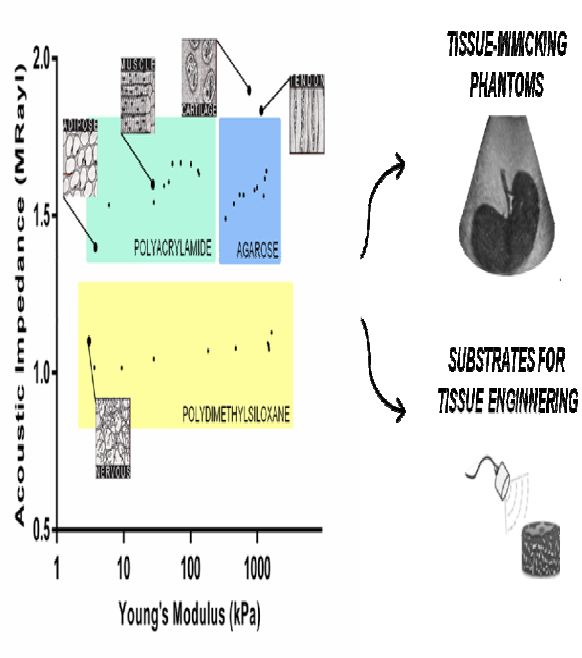

This study reports for the first time the results of a systematic acoustic characterization of agarose, polyacrylamide and polydimethylsiloxane at different concentrations and cross-linking extents and doped with different concentrations of barium titanate nanoparticles. These results can be used to build tissue-mimicking phantoms, useful for many ultrasound-based medical procedures, and to fabricate smart materials for stimulating cells with a highly controlled ultrasound dose.
Thanks to this knowledge, we correlated for the first time a bioeffect (the proliferation increase) on human fibroblasts, triggered by piezoelectric nanoparticles, with a precise US dose delivered. These results may open new avenues for the development of both tissue-mimicking phantoms and smart triggerable scaffolds for tissue engineering and regenerative medicine.